DRUG DELIVERY

Snake fang–inspired stamping patch for transdermal delivery of liquid formulations

Won-Gyu Bae[1]*, Hangil Ko[2], Jin-Young So[1], Hoon Yi[2], Chan-Ho Lee[1], Dong-Hun Lee[3], Yujin Ahn[4], Sang-Hyeon Lee[2], Kyunghun Lee[2], Joonha Jun[1], Hyoung-Ho Kim[5], Noo Li Jeon[6], Woonggyu Jung[4], Chang-Seon Song[7], Taesung Kim[2], Yeu-Chun Kim[8], Hoon Eui Jeong[2]*

A flexible microneedle patch that can transdermally deliver liquid-phase therapeutics would enable direct use of existing, approved drugs and vaccines, which are mostly in liquid form, without the need for additional drug solidification, efficacy verification, and subsequent approval. Specialized dissolving or coated microneedle patches that deliver reformulated, solidified therapeutics have made considerable advances; however, microneedles that can deliver liquid drugs and vaccines still remain elusive because of technical limitations. Here, we present a snake fang–inspired microneedle patch that can administer existing liquid formulations to patients in an ultrafast manner (<15 s). Rear-fanged snakes have an intriguing molar with a groove on the surface, which enables rapid and efficient infusion of venom or saliva into prey. Liquid delivery is based on surface tension and capillary action. The microneedle patch uses multiple open groove architectures that emulate the grooved fangs of rear-fanged snakes: Similar to snake fangs, the microneedles can rapidly and efficiently deliver diverse liquid-phase drugs and vaccines in seconds under capillary action with only gentle thumb pressure, without requiring a complex pumping system. Hydrodynamic simulations show that the snake fang–inspired open groove architectures enable rapid capillary force–driven delivery of liquid formulations with varied surface tensions and viscosities. We demonstrate that administration of ovalbumin and influenza virus with the snake fang–inspired microneedle patch induces robust antibody production and protective immune response in guinea pigs and mice.

INTRODUCTION

Transdermal drug delivery using microneedle (MN) patches has emerged as an attractive alternative to hypodermic injections because it enables simple and painless administration of drugs and vaccines into a patient's skin with minimal risk of needle-associated infection (1–12). MNs coated with or encapsulating drugs in a thin, flexible patch have been extensively studied and have produced considerable advances in related fields, demonstrating advantages such as controlled drug release, efficacious therapy, ease of use, and low fabrication cost (3, 13–18). In combination with rapidly developing skin-attachable flexible electronics techniques, these solid MN patches are now incorporating various advanced therapeutic and diagnostic functions in flexible patch configurations (13). Despite these advances, however, dissolving or coated MNs cannot deliver liquid drug formulations and require additional processing using stabilizers and adjuvants to reformulate liquid drugs as solid products, whereas most existing formulations of drugs and vaccines are in liquid form (1, 3, 4, 19). Solidification of the liquid formulations for the dissolving or coated MNs can reduce formulation activity (vaccine activity) (20).

The viscosity and surface energy of the formulations must also be delicately modulated within a narrow range for successful molding or coating during the manufacture of the dissolving or coated MNs. Furthermore, the reformulation and solidification of liquid formulations require additional efficacy verification and subsequent regulatory approval, thereby limiting the widespread use of MN platform in the clinical setting.

Hollow MNs have been developed for the delivery of liquid therapeutics, but they typically require complex and expensive microelectromechanical systems processes for fabrication, and a bulky pump is required for drug infusion (8, 21–25). They are therefore difficult to prepare in a simple and flexible patch-type configuration, which hinders their clinical use and limits their integration with wearable health care devices. Forced drug infusion by an external pump can induce a backflow of the injected formulation and can be painful for the patient (8, 21–25). A simple and universal patch-type MN platform that can directly deliver liquid therapeutics and vaccines represents an unmet technical goal. Successful development of such an MN platform optimized for the efficient transdermal delivery of diverse liquid therapeutic agents not only would enhance the adoption of MN platform in clinical practice but also could provide simple, timely, and safe preventive measures against highly pathogenic and chronic diseases.

Inspired by the fangs of snakes, here, we report a patch-type MN platform that can deliver a variety of existing liquid drugs and vaccines into the skin in seconds by simply stamping the MN patch against the skin with gentle thumb pressure. This method does not require liquid drug reformulation or a complex pumping system. Our MN platform contains multiple open grooves on its surface that mimic the monogrooved fangs of rear-fanged snakes. Hydrodynamic simulations show that the grooves enable rapid capillary force–driven delivery of liquid formulations. The fang-inspired MN stamping patch with multiple grooves was used to deliver fluorescein isothiocyanate–conjugated

[1]Department of Electrical Engineering, Soongsil University, Seoul 06978, Republic of Korea. [2]Department of Mechanical Engineering, Ulsan National Institute of Science and Technology (UNIST), Ulsan 44919, Republic of Korea. [3]Department of Pathobiology and Veterinary Science, University of Connecticut, Storrs, CT 06269, USA. [4]Department of Biomedical Engineering, Ulsan National Institute of Science and Technology (UNIST), Ulsan 44919, Republic of Korea. [5]Department of Mechanical Engineering, Soongsil University, Seoul 06978, Republic of Korea. [6]School of Mechanical and Aerospace Engineering, Seoul National University, Seoul 08826, Republic of Korea. [7]Avian Disease Laboratory, College of Veterinary Medicine, Konkuk University, Seoul 05029, Republic of Korea. [8]Department of Chemical and Biomolecular Engineering, Korea Advanced Institute of Science and Technology (KAIST), Daejeon 34141, Republic of Korea.
*Corresponding author. Email: hooneejeong@unist.ac.kr (H.E.J.); wgbae@ssu.ac.kr (W.-G.B.)

Bae et al., Sci. Transl. Med. 11, eaaw3329 (2019)   31 July 2019

1 of 11

bovine serum albumin (FITC-BSA) and lidocaine into mouse skin and to vaccinate guinea pigs and mice with ovalbumin or an inactivated pandemic influenza virus, inducing robust antibody production and a protective immune response.

RESULTS

Design of the skin-penetrating snake fang–inspired stamping patch with multiple grooves

Rear-fanged snakes have a venom delivery system that can quickly inject venom or saliva into tissue, although the Duvernoy's gland in these snakes is not able to produce high pressure for delivery (26, 27). The structure of the molars in rear-fanged snakes confers their rapid injection ability (Fig. 1A). The fangs have an open groove on the surface that forms a conduit called a venom tube as the fang penetrates the prey animal's skin. Liquid venom from the Duvernoy's gland runs along the groove and flows into the skin through the venom tube to minimize its surface energy (28). As a result, the venom can be rapidly and efficiently delivered into the prey's tissue, without the need for a high-pressure system. In contrast, front-fanged snakes usually have hollow-tube fangs and exert high pressure from a venom gland to inject venom into their prey (29). Traditional hypodermic needles and hollow MNs are based on the same delivery mechanism as the front-fanged snake. Although this pressure-driven mechanism enables quick delivery of liquid formulations, it typically requires a strong external driving force for injection (a venom gland, actuator, or pump). The narrow tip of the tubular structure can be compressed or clogged by the dense dermal or epidermal tissue of the prey's or patient's skin, necessitating pressure to overcome blockages.

Inspired by the simple and rapid venom delivery mechanism of rear-fanged snakes, we devised an MN stamping patch that has open grooves on the surface (Fig. 1B). These grooves allow liquid drugs or vaccines to be efficiently delivered into the skin without the application of high pressure, enabling spontaneous flow driven by surface tension and capillary force (28). We designed the MN so that liquid formulations can flow down the grooves of the needles and subsequently trickle into the holes formed in the skin. Whereas a snake fang has a single groove, we engraved multiple grooves onto the surface of each needle to enhance the rate of drug delivery. The multigrooved MN (MG-MN) was fabricated by backside exposure lithography using poly(ethylene glycol) diacrylate (PEG-DA) (30). PEG-DA was used because it is biocompatible and has sufficient mechanical strength for skin penetration (31–33). It can also be rapidly cured under ultraviolet (UV) light, which enables the low cost and scalable fabrication of the MG-MN (32, 34). The resulting MG-MNs are 530 to 635 μm in height, 250 μm in base diameter, and 5 μm in top radius of curvature.

Figure 1 (C and D) shows the integrated MG-MN stamping patch, which comprises two main parts: a polydimethylsiloxane (PDMS) chamber and an MN array (see figs. S1 and S2 for details of the fabrication process). The PDMS chamber acts as a drug reservoir similar to the glands of venomous snakes. The reservoir is designed to contain 2 μl of liquid drug formulation; its capacity can be easily modulated by altering the chamber geometry. For example, a reservoir that is 10 mm (width) by 10 mm (depth) by 1 mm (height) could accommodate 100 μl of the liquid formulation. Any injectable liquid drug, biotherapeutic agent, or vaccine can be loaded into the drug chamber through the inlet of the reservoir (Fig. 1D). The MG-MNs were formed over a thin PEG-DA film containing microholes (diameter, 20 μm) through which liquid formulations can flow out of the reser-

voir. When the MG-MNs are inserted into the skin with gentle pressure from a thumb, the liquid drugs from the reservoir flow down the groove and subsequently run into the skin through capillary action. The overall drug delivery mechanism of the MG-MN closely resembles the envenomation mechanism of rear-fanged snakes.

To examine the ability of the MG-MN stamping patch to penetrate the skin, the needle array was inserted into the dorsal skin of mice in vivo under gentle thumb pressure, and the cross-section of the skin was examined using optical coherence tomography (OCT) and histological sectioning. An OCT image of the skin cross section showed that the MG-MNs pierced the stratum corneum (SC) and uniformly penetrated the skin (Fig. 1E). The MG-MN could form a microscale conduit in the skin for transdermal FITC-BSA delivery (Fig. 1F). The MG-MNs were also applied to human and porcine skin, which are thicker than murine skin (35). Uniform penetration and formation of microscale channels in the skin were observed (fig. S3).

Liquid drug delivery performance of the MG-MNs

The multiple grooves on the surface of the MG-MNs provide multiple flow paths to enable rapid, efficient drug delivery. To optimize the design of the MG-MNs, we prepared MNs with different numbers of grooves: tri-, tetra-, penta-, and hexa-grooved MNs (Fig. 2, A to C, fig. S4, and movie S1). All bases of the MG-MNs were designed to be inscribed in a circle 250 μm in diameter (Fig. 2A); however, the MNs differed in height (Fig. 2B). MNs with more grooves were taller than those with fewer grooves: 530, 575, 600, and 635 μm in height for the tri-, tetra-, penta-, and hexa-grooved MNs, respectively. This variation was caused by the different slit areas of the photomasks used to fabricate the MNs (30). The resulting MNs comprise two distinct parts (Fig. 2B): a nongrooved tip that first pierces the skin and a grooved wing that forms a conduit with the wall of the incised skin (drug channel). To characterize the penetration and cargo delivery of the MNs relative to the number of grooves, optical imaging of the MG-MNs inserted into the dorsal skin of a mouse to deliver FITC-BSA was conducted with a confocal microscope and optical coherence microscope (Fig. 2, D to H, and figs. S5 to S7). A three-dimensional (3D) reconstruction of the confocal imaging data showed that the tip of the MN (red), rather than the entire MN, primarily penetrates the skin across the SC (blue) because of deformation of the skin (Fig. 2, F to H, and movie S2). FITC-BSA (green) was observed along the drug channel formed by the MG-MNs and the tissue, which demonstrates that the transdermal delivery of liquid formulations is possible when using the MG-MNs, as we intended (Fig. 2, E to G).

In contrast to the relationship between the number of grooves and height, MNs with more grooves had shorter grooves (Fig. 3A). The length of the tip and the length of the groove are important factors for obtaining proper skin piercing and drug delivery. Because MNs with more grooves have longer tips, piercing of the skin is maximized with the hexa-grooved MN (360 μm), and it is minimized with the tri-grooved MN (179 μm) (Figs. 2H and 3B). Top views of the confocal microscopy and optical coherence microscopy (OCM) images also showed that different hole formations were created in the skin depending on the type of MN inserted. MNs with more grooves created larger holes in the skin because of the deeper penetration (Figs. 2, D and E, and 3C). Different drug channels were observed for different MG-MNs. For example, the tri-grooved MN could only create a small gap in the skin, and FITC-BSA was observed only within a very narrow region around the MN. By contrast, FITC-BSA was observed in a broader vicinity surrounding the penta- and hexa-grooved
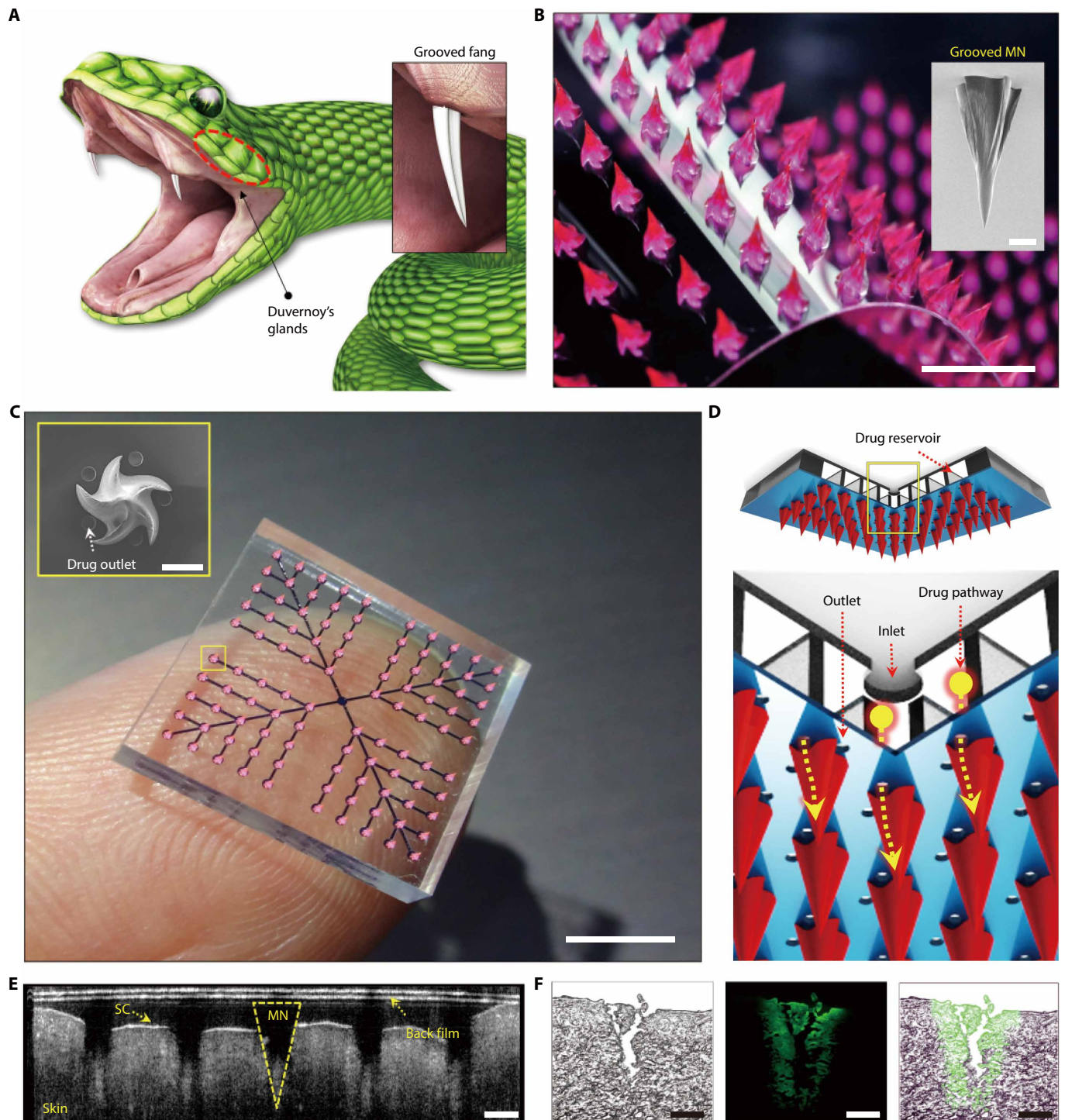
Fig. 1. Design of the snake fang–inspired stamping patch. (**A**) Illustrations of the venom delivery system of the rear-fanged snake. Venom from the Duvernoy's gland runs along the grooved fang and rapidly flows, under capillary action, into the tissue of the prey. (**B**) Photograph of the snake fang–inspired MN array. The inset shows a scanning electron microscopy image of the MG-MN, which has two distinct parts: a nongrooved tip and a grooved wing. After the nongrooved tip pierces the skin, the grooved wing forms a conduit with the wall of the incised skin. (**C**) Photograph of the integrated MN patch held on a human fingertip. The patch consists of an MN array and a PDMS chamber. The inset shows an MN formed over a thin PEG-DA film that has microholes (diameter, 20 μm) through which liquid formulations can trickle out of the chamber (drug outlet). (**D**) Conceptual diagrams of the patch. Liquid drugs are loaded into the chamber through the inlet of the reservoir before use. When the patch is applied over the skin with gentle pressure from a thumb, liquid drugs loaded in the reservoir roll down the grooves (yellow arrows) and enter the skin by capillary action. (**E**) OCT image of a cross section of the dorsal skin from a mouse that was injected with the MN array. The image indicates uniform penetration of the array into the skin through the SC. (**F**) Bright-field, fluorescence and merged micrographs (from left) of a histological section of mouse skin after insertion and removal of an MN patch loaded with FITC-BSA. Scale bars, 300 μm (B); 100 μm (B, inset); 5 mm (C); 100 μm (C, inset); 300 μm (E); and 300 μm (F).
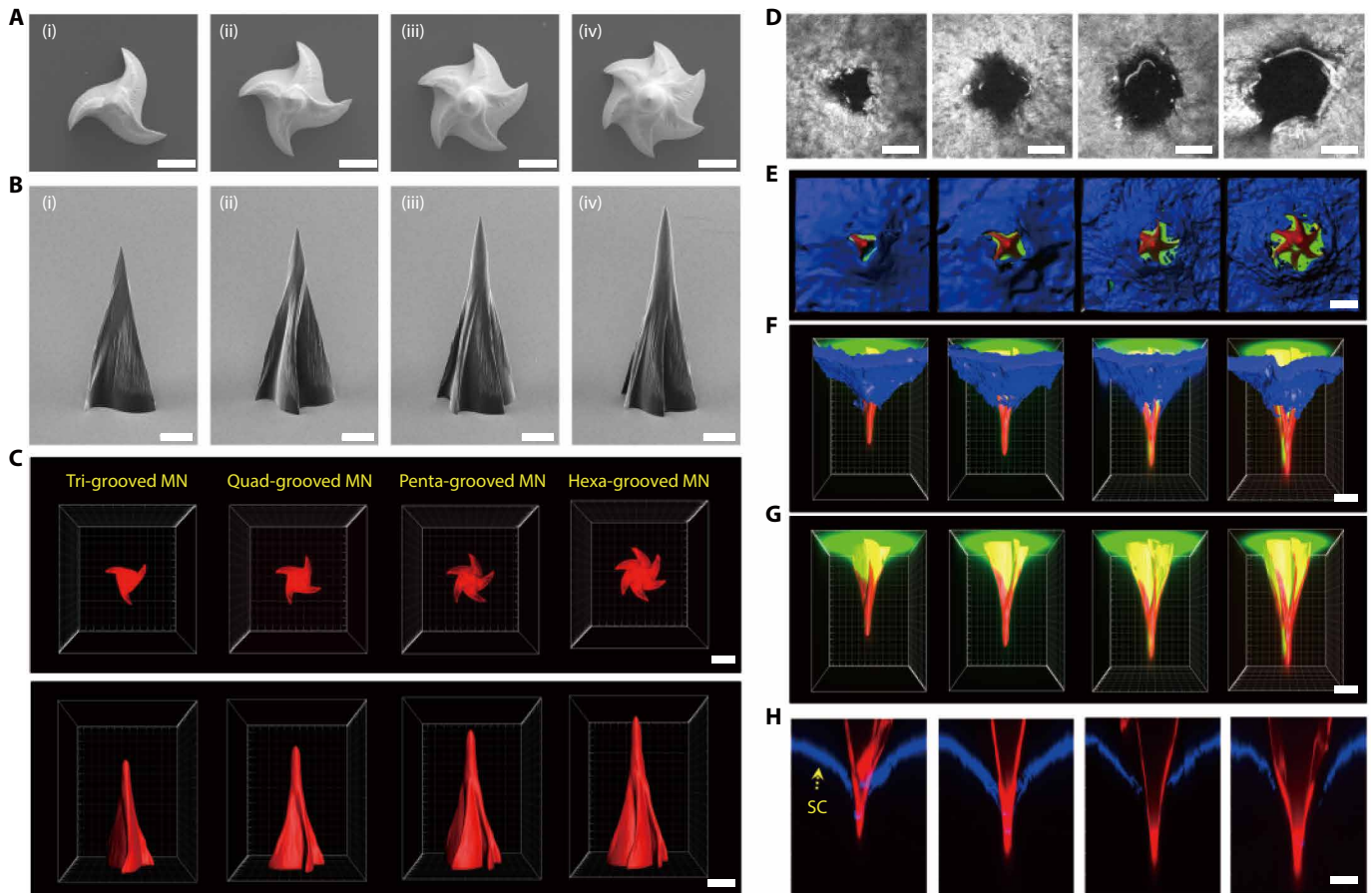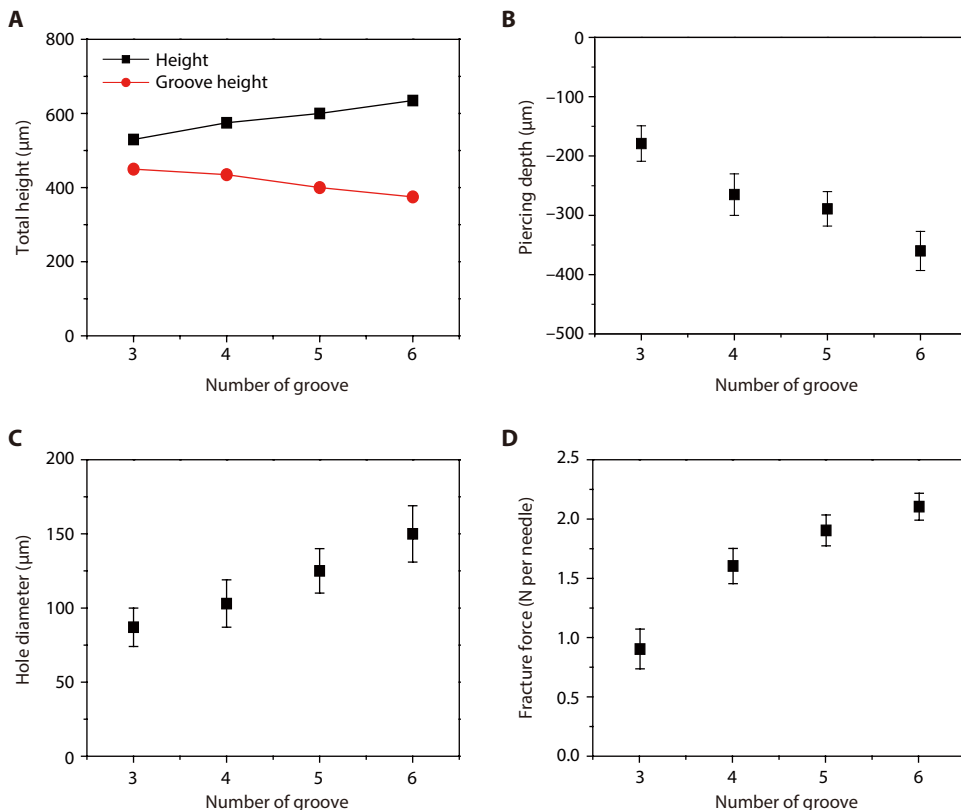
Fig. 2. Rational design of MG-MNs for the transdermal delivery of liquid drugs. (**A** and **B**) Scanning electron microscopy images of the top (A) and side (B) views of (i) tri-grooved, (ii) tetra-grooved, (iii) penta-grooved, and (iv) hexa-grooved MNs. (**C**) 3D reconstruction images of confocal micrographs of MG-MNs. Top row shows top view; bottom row shows side view. (**D**) Top views of OCM micrographs showing the different types of holes created in mouse skin by MNs with different numbers of grooves. (**E** to **H**) Top views (E), side views (F and G), and cross-sectional views (H) of confocal micrographs showing the penetration of MNs (red) with different numbers of grooves loaded with FITC-BSA (green) into the dorsal skin of mice across the SC (blue). The SC is removed in (G) to better visualize the delivery of FITC-BSA into the skin. Scale bars, 100 μm (A to H).

MNs, showing that the penta- and hexa-grooved MNs can generate multiple channels with large effective radii in the skin (Fig. 2E). Different MG-MNs also exhibited different mechanical strengths. The fracture force was greater for the MNs with more grooves: 0.9 and 2.1 N per needle for the tri- and hexa-grooved MNs, respectively (Fig. 3D). This indicates that the MG-MNs are robust enough to penetrate the skin without structural fracture regardless of the number of grooves (fig. S8). Consequently, the hexa-grooved MN has the greatest piercing depth, drug channel diameter, and fracture strength. However, it has the shortest groove; the groove length plays an important role in guiding liquid into the skin. The deeper penetration depth of the hexa-grooved MN could also result in pain (*36*). To avoid this, we used the penta-grooved MN for the in vivo tests performed in this study. The penta-grooved MN has a proper penetration depth for painless insertion and a sufficient channel size and groove length for efficient drug delivery. It also has high mechanical strength.

Hydrodynamic simulation of liquid drug delivery in the MG-MNs

To understand the hydrodynamic behavior of liquid-phase drugs in the MG-MN, we performed computational fluid dynamics simulation using COMSOL Multiphysics with the two-phase flow module in

which the Navier-Stokes equation and a level set method are coupled. Our hydrodynamic simulation results showed that transdermal delivery occurred in an ultrafast manner with the aid of a capillary force caused by the groove structure of the MG-MN. Figure 4 (A and B) shows the schematics of a single groove of the MG-MN inserted into the skin. Once the MG-MN pierces the skin and penetrates the tissue, the groove of the MN and the cut and exposed side of the tissue form an upper wide and lower narrow channel through which a drug droplet can be delivered (Fig. 4, A and B). Figure 4 (C and D) shows the time-lapse drug delivery process and velocities of a liquid droplet in the groove, respectively (movie S3). Initially, under gentle thumb pressure, the droplet moves slowly along the open groove toward the entrance of the closed channel. However, as soon as the droplet reaches the entrance of the closed channel, the velocity sharply increases up to 0.46 m s^{-1}. This increase occurs because the leading (lower) edge of the tube produces a much stronger capillary force than the following (upper) edge that remains outside the tube (*37*, *38*). In addition, when the MN partially penetrates the skin, a closed channel is formed by the MN groove and the tissue, while an open channel is also formed by the upper part of the groove and the air. This contributes to the low-pressure drug delivery that is achieved by our MG-MN stamping patch: The MN has an extensive surface

Fig. 3. Skin-penetration performance of MG-MNs. (A) Total height and groove height of various MG-MNs. (**B** and **C**) Pierced depth (B) and hole diameter (C) in mouse skin for different types of MG-MNs. (**D**) Fracture forces of MNs with different numbers of grooves. Data represent means ± SD (*n* = 5).

droplets with two and five times viscosities. These results indicate that our MG-MN stamping patch can deliver diverse liquid-phase therapeutic agents with varied surface tensions and viscosities, using surface tension and capillary action without necessitating a complex pumping system.

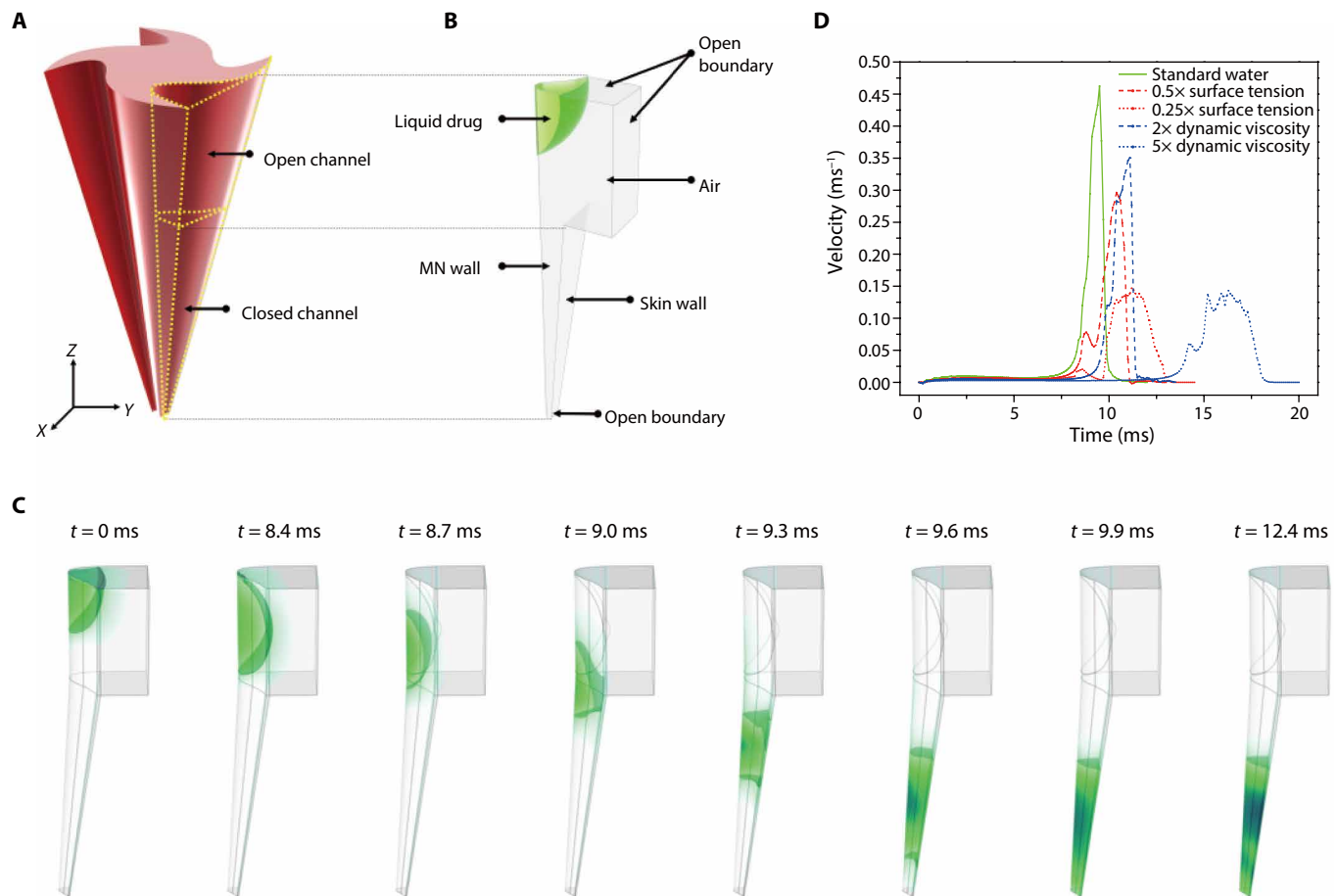### In vivo transdermal delivery of liquid formulations with the snake fang–inspired stamping patch

Transdermal liquid drug delivery using the MG-MN stamping patch was tested in vivo in mice using FITC-BSA–loaded patches (Fig. 5, A and B). Fluorescence images taken after applying the stamping patch for different lengths of time showed that FITC-BSA was delivered into the skin of mice within seconds of insertion (<15 s; Fig. 5, A and B). Direct comparison of the relative fluorescence intensities indicated that prolonged MN insertion was beneficial: More liquid was delivered into the skin with extended contact. A sevenfold increase in photons was detected after 15 s of insertion compared to 5 s of insertion (Fig. 5C). Although the liquid drug delivery from the MN reservoir occurs rapidly, drug absorption into the tissue takes time. Quantitative fluorescence image analysis of histological sections of the penetration sites further confirmed that longer insertion times allowed more FITC-BSA to diffuse into the skin (Fig. 5, B and D). Nonetheless, FITC-BSA could be delivered into the skin within 15 s using the MG-MN patch.

We also examined the diffusion of drug into the skin. Figure 5 (E and F) shows fluorescence images taken before and after a 15-s injection of the FITC-BSA–loaded MN stamping patch. The fluorescence intensity of FITC-BSA immediately after MN removal was similar to the intensity before removal. The intensity decreased over the course of 15 min after the removal of the patch, which indicates that the delivered FITC-BSA gradually diffused into the skin of the mice (Fig. 5, F and G). To further demonstrate the efficacious delivery of clinically relevant liquid formulations, we administered lidocaine, a widely used local anesthetic, to mice using the stamping patch. A 2-µl dose of 4% lidocaine was administered to mice using different insertion durations, and the amount of drug delivered for each duration was quantified using high-performance liquid chromatography (HPLC). As shown in Fig. 5H, 13.35, 33.94, and 141.01 µg cm^{-2} of lidocaine were detected in the skin corresponding to insertion times of 5, 10, and 15 s, respectively, which demonstrates that an anesthetic agent can be rapidly deployed to the skin using an MG-MN stamping patch.

Vaccination with the snake fang–inspired stamping patch

To assess the effectiveness of vaccinations using the MG-MN stamping patch, we investigated humoral immune responses after MN vaccination. MG-MN patches loaded with 2 µl of ovalbumin

area that is exposed to the tissue and the air. Only the tip of conventional hollow MNs and hypodermic needles is exposed to the tissue, requiring a strong external force for injection.

We also investigated the effects of surface tension and viscosity of the liquid droplet on the drug delivery process. Figure 4D shows the calculated velocities of droplets with 0.5× and 0.25× smaller surface tension values compared to that of water. As shown, before the droplet approaches the entrance of the closed channel, the droplet velocities are similar to each other regardless of the surface tension values. When the droplets with smaller surface tension contact to the entrance of the closed channel, their velocities rapidly increase (as with the case of the water droplet). However, the peak velocities of the droplets are relatively smaller (0.3 and 0.15 m s^{-1} for drops with 0.5× and 0.25× surface tension, respectively) compared to that of the standard water drop (0.46 m s^{-1}), which can be easily understood by considering the fact that surface tension is the most important factor for the capillary motion of liquid droplet in microscale channels. Nonetheless, the enhanced velocities of the liquid droplets in the closed channel are ~2 orders higher than velocities in the open channel. In addition to the surface tension, we also investigated the effects of drop viscosity on the drug delivery process in the MG-MN. As shown in Fig. 4D, when the viscosity of the droplet is two or five times higher than that of a water droplet but other properties remain constant, the droplet takes a longer time to reach the entrance of the closed channel. Viscous shear stresses on the droplet induced by the wall are proportional to the viscosity of the droplet; however, once the droplet reaches the closed channel, the droplet velocity sharply increases for

Fig. 4. Simulation of hydrodynamics of liquid drug delivery in MG-MNs. (**A**) Schematic illustration of MG-MNs having upper wide and lower narrow channels through which a liquid droplet is delivered. (**B**) Schematic of the simulation model of the drug delivery process in a single groove of MG-MNs inserted into the skin. (**C**) Time-lapse simulation results of a water droplet that initially moves slowly and then rapidly passes through the channel enclosed by an MN wall and skin tissue. (**D**) Calculated moving velocities of droplets with different fluid properties during the drug delivery process.

antigen (OVA) without adjuvants were applied to the dorsal skin of guinea pigs ($n = 10$) for two different insertion times, 5 and 15 s (Fig. 6A). The same dose of OVA was administered to guinea pigs via intramuscular injection for comparison, and a 2-μl aliquot of phosphate-buffered saline (PBS) was injected using MNs as a control. Analysis of anti–OVA-specific immunoglobulin G (IgG) 14 and 28 days after immunization using enzyme-linked immunosorbent assay (ELISA) showed enhanced OVA-specific IgG titers in all groups except the control (Fig. 6A). In particular, guinea pigs immunized with the MG-MNs (15 s of insertion) showed enhanced OVA-specific IgG titers compared to intramuscularly immunized guinea pigs. We hypothesize that this is because a large number of immunologically active cells and antigen-presenting cells (APCs) exist in the epidermis or upper layers of the dermis (*39–41*). Therefore, MN-based skin vaccination can potentially result in stronger immune responses with lower antigen concentrations (so-called dose-sparing effect) compared to the traditional intramuscular vaccination (*42–45*). Such dose-sparing can compensate for the limited injection volume capacity of the MN platform compared to that of the conventional hypodermic needle injection. The MG-MN injections administered for 15 s also induced higher IgG titers than the injection case for 5 s, which is consistent with the results shown in Fig. 5. OVA-specific IgG titers

were reduced for all groups on day 28, although the MN-immunized groups still showed higher IgG titers compared to other groups.

To further explore the potential of the MG-MN stamping patch as a tool for vaccination, we administered inactivated pandemic/2009 H1N1 influenza virus (pH1N1) to mice ($n = 10$) via MG-MN or intramuscular injections, and we analyzed the hemagglutination (HA) inhibition (HI) titers in the mice. Compared to the control group, all immunized groups showed enhanced HI titers 14 and 28 days after immunization (Fig. 6B). MN immunization with 5 s of insertion resulted in much lower HI titers than intramuscular injection. In contrast, immunization with MNs for a longer insertion time (15 s) induced higher HI titers than those induced by intramuscular vaccination. This result agreed with those of prior studies reporting enhanced immune responses of MN influenza vaccination compared to the intramuscular vaccination because of the dose-sparing effect caused by the higher number of APCs in the skin (*43–45*). The difference in the immune responses between the 5-s OVA-treated group (Fig. 6A) and the 5-s pH1N1-treated group (Fig. 6B) could have originated from the different immunogenicity degrees of the vaccines (*46, 47*). To validate the immunogenicity and protective efficacy of the influenza immunization, we challenged the immunized groups with lethal influenza virus 4 weeks after the vaccination. The control

Bae *et al.*, *Sci. Transl. Med.* **11**, eaaw3329 (2019) 31 July 2019

6 of 11
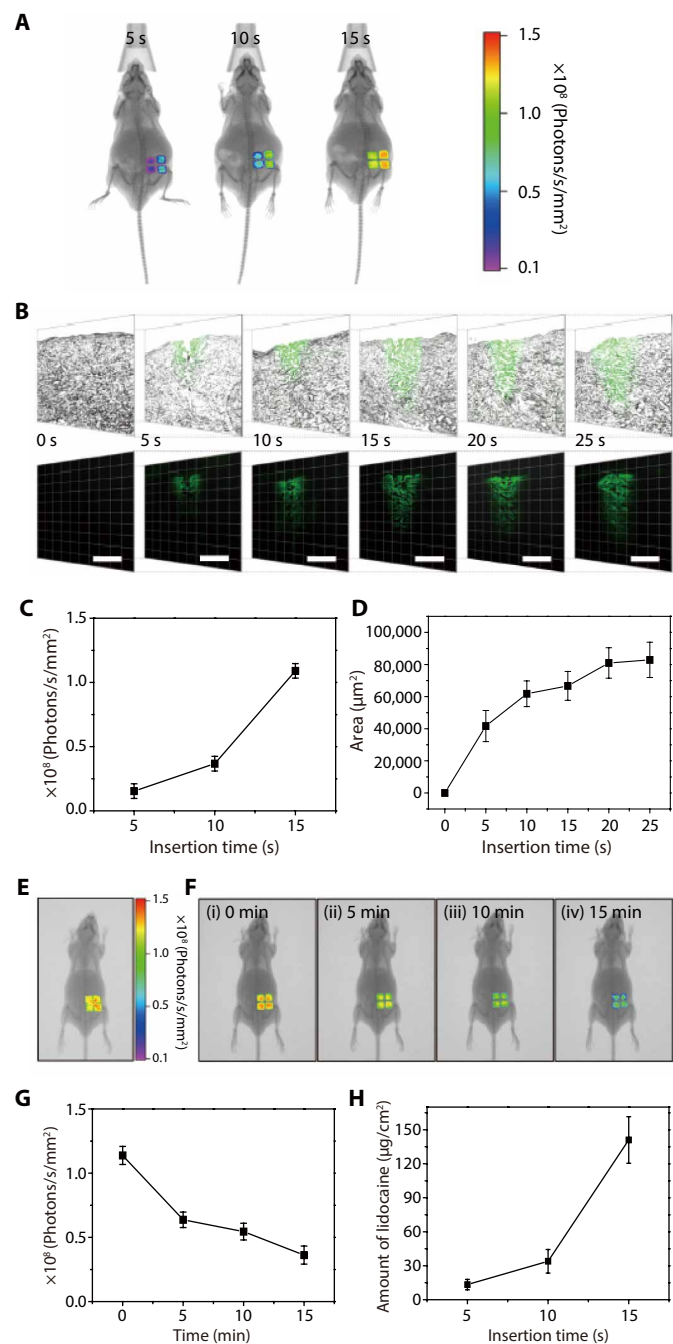
Fig. 5. In vivo transdermal delivery of FITC-BSA and lidocaine into mice using MG-MN patches. (**A**) In vivo fluorescence images taken after applying an MG-MN patch loaded with FITC-BSA onto the dorsal skin of mice for different MN insertion times. (**B**) Merged (bright field + fluorescence, top row) and fluorescence (bottom row) micrographs of histological sections of the pierced murine skin for different insertion times. The images were taken after removal of the MN. FITC-BSA is indicated in green. (**C** and **D**) Quantitative analysis of fluorescence intensity of FITC-BSA in the in vivo test (C) and the diffusion area of FITC-BSA during the test (D). (**E** and **F**) In vivo fluorescence images before (E) and after (F) removal of the FITC-BSA–loaded patch. The MN insertion time was 15 s in this experiment. (**G**) Quantitative analysis of fluorescence intensity of FITC-BSA in the in vivo test (F). (**H**) The amounts of lidocaine delivered into the skin for different insertion times, quantified using HPLC. Scale bars, 100 μm (B). Data represent means ± SD (n = 5).

(unimmunized) group exhibited a sharp decrease in body weight after exposure to the pH1N1 and did not survive more than 8 days after exposure (Fig. 6, C and D). In contrast, a single administration of the vaccine with an MN patch with an insertion time of 15 s protected all of the mice against the lethal exposure to the virus, and the mice recovered their normal body weight after an initial reduction. This shows that our MG-MNs not only enable simple and fast vaccination but also induce robust protective immune responses with a single administration.

DISCUSSION

Over the past few decades, MN technology has rapidly evolved, and translation of the MN technology into the clinical setting is now of immense interest in this field (42, 48). To translate the MNs, a number of issues must be considered, including the scalable aseptic manufacturing of MNs, adopting a patient-friendly and error-free MN insertion method, consequences of deposition of MN residues in the skin, and the storage stability of MNs (42). Regarding the scalable and aseptic production issue, compared to silicon MNs that require multiple fabrication steps and clean room facilities or dissolving MNs that require relatively long solidification times, our MG-MN has advantages in that the MN array can be fabricated within a few tens of seconds using UV-curable and biocompatible PEG-based polymer. However, our MN requires an additional drug chamber, whereas dissolving MNs load drugs or vaccines in the MN body itself without the need for the chamber, which would potentially increase the fabrication cost. For patient safety, sterilization of the MNs is essential during manufacturing. According to a previous study, sterilization of MNs by γ-irradiation, steam autoclave, or microwave heating could damage the cargos loaded within them (49). Therefore, for our MG-MNs, the drugs or vaccines must be loaded in the chamber after sterilization of the MN device.

Consistent skin insertion with intuitive patient-friendly feedback also requires consideration. Although diverse applicators have been devised to enhance the consistency in the MN skin insertion with feedback functions, their use is less patient friendly and would increase the product cost. In contrast, although manual insertion is simple, it would increase the interindividual variability in skin insertion. It can also be difficult for patients to ensure that they properly apply MNs to the skin (50). For our MNs, patients could perceive the proper delivery of the drugs or vaccines by observing the elevation of the residual liquid formulations in the chamber. However, incorporating a more intuitive feedback mechanism into the device would enhance patient compliance. To this end, a low-cost pressure-indicating sensor film (PISF) can be assembled over the chamber of the MG-MN because of its simple and flexible thin film architecture (50). The PISF exhibits colorations in response to external pressure application. Vicente-Pérez et al. (50) successfully demonstrated that the simple incorporation of the PISF into their hydrogel-forming MN could provide appropriate feedback to patients to guarantee proper insertion with minimal cost. The deposition of MN residues into the skin could lead to adverse effects in the patient skin, a consideration for dissolving MNs. Unlike the dissolving MNs, our MG-MN did not appear to leave any MN residue in the skin upon its removal after a few or a few tens of seconds of skin insertion. However, this also indicates that the MG-MN may not be appropriate for a prolonged long-term cargo delivery. For controlled long-term cargo delivery using our MNs, microfluidic components such as valves
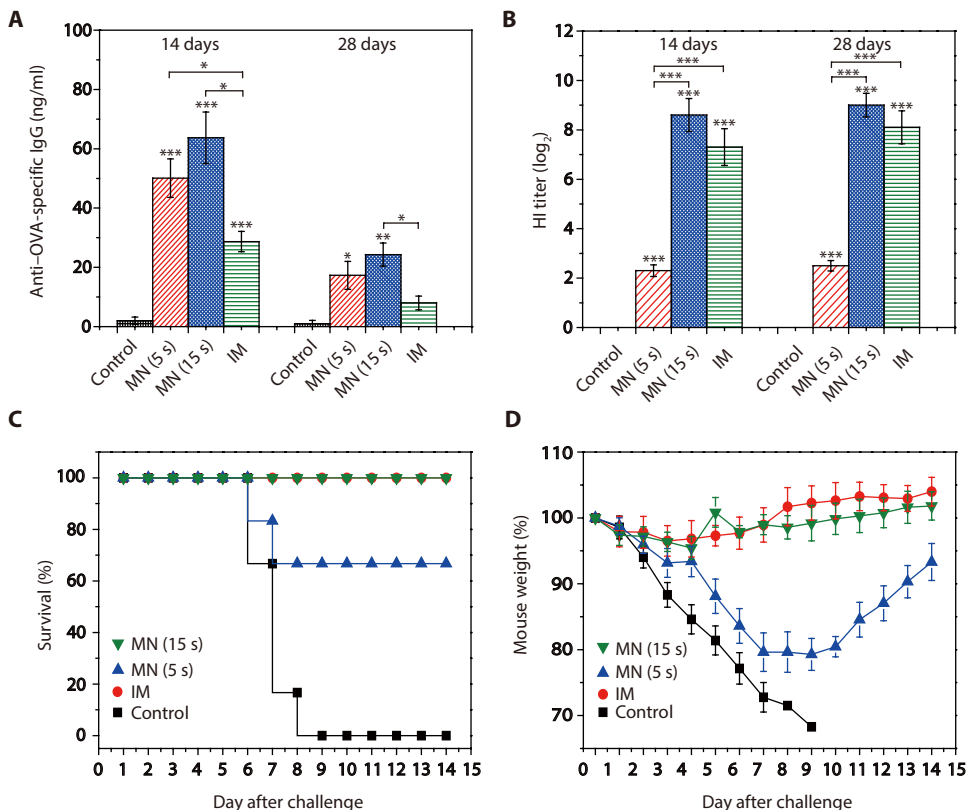
Fig. 6. Vaccination using MG-MN patches. (**A**) Anti–OVA-specific IgG titers from guinea pigs, analyzed using ELISA, 14 and 28 days after immunization. MN patches loaded with 2 μl of OVA were applied to the dorsal skin of guinea pigs ($n = 10$) for two different insertion times: 5 and 15 s. The same dose of the OVA was administered to guinea pigs via intramuscular (IM) injection for comparison. A 2-μl dose of PBS was injected with the patch as a control. (**B**) HI titers of mice ($n = 10$) after administration of pH1N1 via MN or intramuscular injection. (**C** and **D**) Survival rate and change in body weight of mice after a lethal exposure to the pH1N1 4 weeks after vaccination. The means and SEM ($n = 10$; *$P < 0.05$, **$P < 0.01$, and ***$P < 0.001$) are shown in all panels (Welch's ANOVA).

would be required to be incorporated into the device. Because our MN devices contain liquid formulations in the chamber, they require cold chain for storage stability as with the storage of conventional liquid formulations, which would potentially limit the use of the MN in developing countries. Additional factors should be carefully considered to improve the MG-MN design toward its translation into clinical practice (*42*).

Hypodermic needle injection for liquid drug or vaccine delivery works well. However, a set of prior studies demonstrated distinct advantages of MN-based delivery over conventional needle injection, including improved patient compliance, acceptability, immunogenicity, and safety (*1*, *42*). Enhanced patient compliance is among the most important aspects of the MN technique because MNs painlessly pierce the epidermis without stimulating dermal nerves in a minimally invasive manner. Because of the enhanced compliance, patients and health care professionals showed positive attitudes about the use of MNs over conventional intramuscular injection in several prior studies (*42*). For example, according to a prior study by Norman *et al.* (*51*), influenza vaccination by MNs instead of hypodermic injection resulted in an increased vaccination intent from 44 to 65%. MN technology is especially useful for patients who require regular repeated drug injection or blood sampling. Norman *et al.* (*52*) reported that the use of hollow MNs for insulin delivery in children

and adolescents with type 1 diabetes noticeably reduced injection pain compared to injection by a subcutaneous catheter. Mooney *et al.* (*53*) reported that child participants showed strong support and enhanced acceptability of MN-based blood sampling compared to sampling using traditional hypodermic needles. Furthermore, a study of MN acceptability by Birchall *et al.* (*54*) reported that public (100%) and health care professional (75%) participants were overall positive in the use of MNs because of the benefits of the MN technology (reduced pain, tissue damage, and risk of infection transmission) compared to conventional needle injections, as well as the potential for self-administration. The positive perception and high acceptability of the MN vaccination from general public and health care professionals were also reported in a study by Arnou *et al.* (*55*). In addition to enhanced patient compliance, MN vaccination leads to a stronger immune response with a lower dose of vaccine compared with the conventional intramuscular injection as described above without the potential dangers of hypodermic needles (*3*). By considering the limited manufacturing and supply capacity of influenza vaccines in the event of a pandemic, the development of an MN-based influenza vaccination is highly desirable as a dose-sparing vaccination strategy (*56*). Such a dose-sparing effect was verified in this study

with the MG-MN as in prior reports (*42–45*).

In the present study, a limited number of liquid formulations (FITC-BSA, lidocaine, OVA, and influenza vaccine) were tested to investigate transdermal liquid drug delivery of the MG-MNs in mice and guinea pigs. Additional studies accessing the efficacy and safety of the MG-MN patch using a wider variety of liquid drugs and vaccines in larger animal models and human participants are required to translate the MG-MN technique to clinical trials. Nonetheless, with its simple fabrication process and rapid liquid drug delivery capability, we expect that this MG-MN technique can provide a valuable platform for the simple, fast, and smart administration of diverse liquid drugs, biotherapeutic agents, and vaccines against diverse pathogenic and chronic diseases.

MATERIALS AND METHODS
Study design
The objective of this study was to investigate the feasibility and efficacy of transdermal delivery of liquid-phase therapeutics and vaccines using MG-MN patches. First, the MG-MNs with four different designs of open grooves (tri-, tetra-, penta-, and hexa-grooved MNs) were prepared, and their skin penetration performances were evaluated using mouse, pig, and human skin and confocal microscopy,

OCM, and OCT analyses. Then, transdermal liquid drug delivery using the MG-MNs was evaluated by the injection of FITC-BSA and lidocaine into live mice. Last, the immune responses of guinea pigs were investigated by the application of OVA-loaded MG-MN to the dorsal skin of guinea pigs for two different insertion times (5 and 15 s). The same dose of OVA was administrated to guinea pigs via intramuscular injection for comparison. The immune responses of mice were also studied by the administration of inactivated pH1N1 to mice via MG-MN or intramuscular injections. A 2-μl aliquot of PBS was injected using MNs as controls. In vivo studies involving OVA vaccination were performed in guinea pigs randomly housed in four groups of 10 guinea pigs each. In vivo studies involving pH1N1 vaccination were performed in BALB/c mice randomly housed in four groups of 10 mice each. The investigators were blinded to group allocation during experiments and data assessment. All animal procedures performed in this study were reviewed, approved, and supervised by the Institutional Animal Care and Use Committee of Konkuk University (permit number KU14123). All experiments on the human participant were approved by the Institutional Review Board (IRB) of the Ulsan National Institute of Science and Technology (IRB number UNISTIRB-18-63-A).

Fabrication of a snake fang–inspired stamping patch
The MG-MN patch comprises two main parts: a PDMS chamber and an MN array.
Preparation of PDMS chamber
The PDMS chamber, which serves as a drug reservoir, was fabricated by replica molding of a patterned silicon master with a PDMS prepolymer (Sylgard 184, Dow Corning). The patterned silicon master was prepared by forming positive microstructures on a silicon substrate with a photolithographic process using SU-8 100 (MicroChem) as a photoresist. Then, PDMS base mixed with a curing agent in a 10:1 weight ratio was poured onto the silicon master. After degassing and thermal curing at 65°C for 2 hours, the cured PDMS was peeled off from the master, resulting in a PDMS drug chamber. A circular hole, which serves as an inlet for loading drugs into the chamber, was formed on the back side of the chamber using a disposable biopsy punch (diameter, 1 mm; Integra Miltex).
Preparation of MN array
The MN array was formed over a thin PEG-DA film containing microholes. The PEG-DA film with microholes was prepared by applying a MIMIC (micromolding in capillaries) technique. A PDMS pillar array (pillar diameter, 20 μm; height, 100 μm) was first prepared using a replica molding process. Then, the PDMS pillar array was placed on a flat PDMS slab. Subsequently, precured PEG-DA (Mn = 250; Sigma-Aldrich) mixed with 0.5 weight % 2-hydroxy-2-methylpropiophenone (Sigma-Aldrich), a water-soluble photoinitiator, was introduced into the gap between the PDMS slab and the pillar array by capillary action. The PEG-DA mixture was cured under UV light (intensity, 20 mJ s^{-1}; exposure time, 30 s). The solidified PEG-DA membrane was peeled off of the PDMS pillar array, resulting in a PEG-DA membrane with holes. MN arrays were fabricated over the PEG-DA membrane by backside exposure lithography. First, the prefabricated PEG-DA membrane was placed and aligned on a photomask with transparent multiple blade patterns (fig. S1, A and B). Then, a coverslip was placed on the PEG-DA membrane at a distance using spacers (thickness, 1 mm) to form a space with uniform thickness in which precured PEG-DA enters through capillary action (fig. S1C). Subsequent UV exposure through the photomask generated MN arrays on the PEG-DA membrane with microholes (fig. S1, D to F). The cured MN array was rinsed with ethanol and deionized water several times and was then dried with a nitrogen gun to remove uncured residual PEG-DA.

Integration of PDMS chamber and MN array
To assemble the PDMS chamber and the MN array, the backside of the PEG-DA membrane was treated with oxygen plasma for 60 s (60 W, PDC-32G, Harrick Scientific) after dehydration at 60°C for 1 hour. A droplet of (3-aminopropyl)triethoxysilane (APTES) (Sigma-Aldrich) was uniformly applied to the backside of the PEG-DA membrane. The surface of the PDMS chamber was also treated with oxygen plasma and then brought in contact with the APTES-treated PEG-DA membrane for irreversible bonding of these two parts, resulting in an integrated MG-MN patch (fig. S1, G to I).

Manual skin penetration tests
The MG-MNs were inserted into the skin of a human volunteer (male, 27 years old), pigs, and mice under gentle thumb pressure, and the cross sections were examined using OCT, OCM, and histological sectioning.

In vivo experiment
Preparation of antigen in mice
pH1N1, A/Korea/01/2009 (H1N1), was propagated in the allantoic cavities of 9- to 11-day-old specific pathogen–free embryonated chicken eggs. Seventy-two hours after inoculation, allantoic fluid containing pH1N1 was harvested and purified by low-speed centrifugation (2000g, 30 min, 4°C), and the pH1N1 from the supernatants was pelleted using ultracentrifugation (30,000g, 1.5 hours, 4°C). The pelleted virus was resuspended in PBS solution (pH 7.4; Thermo Fisher Scientific) and purified using 20 to 50% (w/v) discontinuous sucrose density gradient purification (150,000g, 2.5 hours, 4°C). The pH1N1 was inactivated by binary ethylenimine. Then, the amount of proteins was measured using a QuantiPro bicinchoninic acid assay kit (Sigma-Aldrich) according to the manufacturer's instructions. Antigens were diluted to solutions of 0.5 μg μl^{-1} for the MN immunization and 0.1 μg μl^{-1} for the intramuscular injection.
Immunogenicity and protective efficacy in mice
Six-week-old female BALB/c mice (Orient Bio) were housed in four groups of 10 mice each: mice that were immunized by MN for 5 s (MN 5 s group), mice that were immunized by MN for 15 s (MN 15 s group), mice that were immunized via an intramuscular route (intramuscular group), and mice that were immunized with PBS (PBS control group). Each mouse in the immunization groups received 1 μg of antigen. Mice were intraperitoneally anesthetized with Avertin (375 mg kg^{-1}). During anesthesia, the hair on the back was removed with a depilatory cream (Veet, Reckitt Benckiser); the back was washed with warm water and 70% ethanol (Sigma-Aldrich) for 5 min after application of the removal cream. Then, the mice in the MN 5 and 15 s groups were immunized with 2 μl of pH1N1 antigen solution by an MN patch for 5 or 15 s, respectively. The mice in the intramuscular group were injected via an intramuscular route with 10 μl of pH1N1 antigen solution. After 4 weeks of immunization, the mice were anesthetized by an intraperitoneal injection of Avertin (375 mg kg^{-1}) and challenged intranasally with 90 μl of 10^6 median embryo infectious dose of pH1N1 for the challenge experiment. The weight and survival rate were monitored for 14 days after the challenge. A body weight loss of more than 25% as compared to the body weight on the day before the challenge was considered to have reached

a humane end point; these mice were euthanized. HI antibody responses in mouse sera collected at 2 and 4 weeks after immunization were measured using an HI test. For the HI assay, serum samples were first treated with a receptor-destroying enzyme (Denka Seiken) by overnight incubation at 37°C and then for 30 m at 56°C. Sera were serially diluted, mixed with 4 HA units of pH1N1, and incubated for 30 m at room temperature before adding 0.5% chicken red blood cells. The reciprocal of the highest serum dilution preventing HA was scored as the HI titer.

Preparation of antigen in guinea pig
Ovalbumin (Sigma-Aldrich) was used as the antigen. Ovalbumin was diluted to solutions of 15 µg µl^{-1} for the MN immunization and 3 µg µl^{-1} for the injection via the intramuscular route using PBS solution.

Immunogenicity and protective efficacy in guinea pig
Five-week-old male guinea pigs weighing 200 to 250 g (Orient Bio) were housed in four groups of 10 guinea pigs each: guinea pigs that were immunized by MN for 5 s (MN 5 s group), guinea pigs that were immunized by MN for 15 s (MN 15 s group), guinea pigs that were immunized via the intramuscular route (intramuscular group), and guinea pigs that were immunized with PBS (PBS control group). Each guinea pig in the immunization groups received 30 µg of OVA. During anesthesia, the hair on the back was removed with a depilatory cream; the back was washed with warm water and 70% ethanol for 5 min after application of the removal cream. Then, the guinea pigs in the MN 5 and 15 s groups were immunized with 2 µl of ovalbumin solution by an MN patch for 5 or 15 s, respectively. The mice in the intramuscular group were injected via an intramuscular route with 10 µl of ovalbumin solution. Serum was prepared, and OVA-specific IgG was measured by ELISA according to the manufacturer's recommendations (catalog number MBS727414, MyBioSource). Samples were analyzed in duplicate, and absorbance was read at 405 nm.

Statistical analysis
Datasets were analyzed using Welch's analysis of variance (ANOVA) test. In all cases, P values of <0.05 were considered statistically significant. Calculations were performed using SPSS version 10.1. Primary data are reported in data file S1.

SUPPLEMENTARY MATERIALS
stm.sciencemag.org/cgi/content/full/11/503/eaaw3329/DC1
Materials and Methods
Fig. S1. Fabrication of the snake fang–inspired MN patch.
Fig. S2. Optimization of UV exposure conditions for the fabrication of MNs with robust structures and sharp tips.
Fig. S3. Penetration of MG-MNs into the human and porcine skin.
Fig. S4. Fabrication of MG-MNs.
Fig. S5. Automated skin penetration test.
Fig. S6. Schematic of the spectral domain OCT system.
Fig. S7. Schematic of the OCM system.
Fig. S8. Mechanical property test of MN arrays.
Data file S1. Primary data.
Movie S1. 3D confocal reconstruction of the hexa-grooved MN.
Movie S2. 3D reconstruction showing the penetration of the hexa-grooved MN (red) loaded with FITC-BSA (green) into the dorsal skin of mice across the SC (blue).
Movie S3. Simulation of liquid drug delivery in a single groove of MG-MN.

REFERENCES AND NOTES
1. M. R. Prausnitz, R. Langer, Transdermal drug delivery. *Nat. Biotechnol.* **26**, 1261–1268 (2008).
2. A. Mandal, A. V. Boopathy, L. K. W. Lam, K. D. Moynihan, M. E. Welch, N. R. Bennett, M. E. Turvey, N. Thai, J. H. Van, J. C. Love, P. T. Hammond, D. J. Irvine, Cell and fluid sampling microneedle patches for monitoring skin-resident immunity. *Sci. Transl. Med.* **10**, eaar2227 (2018).
3. S. P. Sullivan, D. G. Koutsonanos, M. del Pilar Martin, J. W. Lee, V. Zarnitsyn, S.-O. Choi, N. Murthy, R. W. Compans, I. Skountzou, M. R. Prausnitz, Dissolving polymer microneedle patches for influenza vaccination. *Nat. Med.* **16**, 915–920 (2010).
4. K. van der Maaden, W. Jiskoot, J. Bouwstra, Microneedle technologies for (trans)dermal drug and vaccine delivery. *J. Control. Release* **161**, 645–655 (2012).
5. J. Yu, Y. Zhang, Y. Ye, R. DiSanto, W. Sun, D. Ranson, F. S. Ligler, J. B. Buse, Z. Gu, Microneedle-array patches loaded with hypoxia-sensitive vesicles provide fast glucose-responsive insulin delivery. *Proc. Natl. Acad. Sci. U.S.A.* **112**, 8260–8265 (2015).
6. H.-W. Yang, L. Ye, X. D. Guo, C. Yang, R. W. Compans, M. R. Prausnitz, Ebola vaccination using a DNA vaccine coated on PLGA-PLL/γPGA nanoparticles administered using a microneedle patch. *Adv. Healthc. Mater.* **6**, 1600750 (2017).
7. O. Veiseh, R. Langer, Diabetes. A smart insulin patch. *Nature* **524**, 39–40 (2015).
8. Y.-C. Kim, J.-H. Park, M. R. Prausnitz, Microneedles for drug and vaccine delivery. *Adv. Drug Deliv. Rev.* **64**, 1547–1568 (2012).
9. W. K. Cho, J. A. Ankrum, D. Guo, S. A. Chester, S. Y. Yang, A. Kashyap, G. A. Campbell, R. J. Wood, R. K. Rijal, R. Karnik, R. Langer, J. M. Karp, Microstructured barbs on the North American porcupine quill enable easy tissue penetration and difficult removal. *Proc. Natl. Acad. Sci. U.S.A.* **109**, 21289–21294 (2012).
10. P. P. Samant, M. R. Prausnitz, Mechanisms of sampling interstitial fluid from skin using a microneedle patch. *Proc. Natl. Acad. Sci. U.S.A.* **115**, 4583–4588 (2018).
11. Y. He, C. Hong, J. Li, M. T. Howard, Y. Li, M. E. Turvey, D. S. S. M. Uppu, J. R. Martin, K. Zhang, D. J. Irvine, P. T. Hammond, Synthetic charge-invertible polymer for rapid and complete implantation of layer-by-layer microneedle drug films for enhanced transdermal vaccination. *ACS Nano* **12**, 10272–10280 (2018).
12. H. Lee, C. Song, Y. S. Hong, M. S. Kim, H. R. Cho, T. Kang, K. Shin, S. H. Choi, T. Hyeon, D.-H. Kim, Wearable/disposable sweat-based glucose monitoring device with multistage transdermal drug delivery module. *Sci. Adv.* **3**, e1601314 (2017).
13. I. Hwang, H. N. Kim, M. Seong, S.-H. Lee, M. Kang, H. Yi, W. G. Bae, M. K. Kwak, H. E. Jeong, Multifunctional smart skin adhesive patches for advanced health care. *Adv. Healthc. Mater.* **7**, 1800275 (2018).
14. M. An, H. P. Liu, Dissolving microneedle arrays for transdermal delivery of amphiphilic vaccines. *Small* **13**, 1700164 (2017).
15. Y. Zhang, J. Wang, J. Yu, D. Wen, A. R. Kahkoska, Y. Lu, X. Zhang, J. B. Buse, Z. Gu, Bioresponsive microneedles with a sheath structure for H$_2$O$_2$ and pH cascade-triggered insulin delivery. *Small* **14**, 1704181 (2018).
16. H. Chang, M. Zheng, X. Yu, A. Than, R. Z. Seeni, R. Kang, J. Tian, D. P. Khanh, L. Liu, P. Chen, C. Xu, A swellable microneedle patch to rapidly extract skin interstitial fluid for timely metabolic analysis. *Adv. Mater.* **29**, 1702243 (2017).
17. J. Yu, C. Qian, Y. Zhang, Z. Cui, Y. Zhu, Q. Shen, F. S. Ligler, J. B. Buse, Z. Gu, Hypoxia and H$_2$O$_2$ dual-sensitive vesicles for enhanced glucose-responsive insulin delivery. *Nano Lett.* **17**, 733–739 (2017).
18. Y. Zhang, Q. Liu, J. Yu, S. Yu, J. Wang, L. Qiang, Z. Gu, Locally induced adipose tissue browning by microneedle patch for obesity treatment. *ACS Nano* **11**, 9223–9230 (2017).
19. G. Valdés-Ramírez, J. R. Windmiller, J. C. Claussen, A. G. Martinez, F. Kuralay, M. Zhou, N. Zhou, R. Polsky, P. R. Miller, R. Narayan, J. Wang, Multiplexed and switchable release of distinct fluids from microneedle platforms via conducting polymer nanoactuators for potential drug delivery. *Sensors Actuators B Chem.* **161**, 1018–1024 (2012).
20. Y.-C. Kim, F.-S. Quan, R. W. Compans, S.-M. Kang, M. R. Prausnitz, Stability kinetics of influenza vaccine coated onto microneedles during drying and storage. *Pharm. Res.* **28**, 135–144 (2011).
21. J. G. E. Gardeniers, R. Luttge, J. W. Berenschot, M. J. de Boer, S. Y. Yeshurun, M. Hefetz, R. van't Oever, A. van den Berg, Silicon micromachined hollow microneedles for transdermal liquid transport. *J. Microelectromech. Syst.* **12**, 855–862 (2003).
22. D. W. Bodhale, A. Nisar, N. Afzulpurkar, Structural and microfluidic analysis of hollow side-open polymeric microneedles for transdermal drug delivery applications. *Microfluid. Nanofluid.* **8**, 373–392 (2010).
23. S. A. Burton, C.-Y. Ng, R. Simmers, C. Moeckly, D. Brandwein, T. Gilbert, N. Johnson, K. Brown, T. Alston, G. Prochnow, K. Siebenaler, K. Hansen, Rapid intradermal delivery of liquid formulations using a hollow microstructured array. *Pharm. Res.* **28**, 31–40 (2011).
24. K. Kim, J.-B. Lee, High aspect ratio tapered hollow metallic microneedle arrays with microfluidic interconnector. *Microsyst. Technol.* **13**, 231–235 (2007).
25. R. F. Donnelly, T. R. R. Singh, A. D. Woolfson, Microneedle-based drug delivery systems: Microfabrication, drug delivery, and safety. *Drug Deliv.* **17**, 187–207 (2010).
26. A. J. Saviola, M. E. Peichoto, S. P. Mackessy, Rear-fanged snake venoms: An untapped source of novel compounds and potential drug leads. *Toxin Rev.* **33**, 185–201 (2014).
27. K. V. Kardong, Colubrid snakes and Duvernoy's "venom" glands. *J. Toxicol.Toxin Rev.* **21**, 1–19 (2002).
28. B. A. Young, F. Herzog, P. Friedel, S. Rammensee, A. Bausch, J. L. van Hemmen, Tears of venom: Hydrodynamics of reptilian envenomation. *Phys. Rev. Lett.* **106**, 198103 (2011).

29. K. V. Kardong, P. A. Lavin-Murcio, Venom delivery of snakes as high-pressure and low-pressure systems. *Copeia* **1993**, 644–650 (1993).

30. J. Onishi, K. Makabe, Y. Matsumoto, Fabrication of micro sloping structures of SU-8 by substrate penetration lithography. *Microsyst. Technol.* **14**, 1305–1310 (2008).

31. J. S. Kochhar, T. C. Quek, W. J. Soon, J. Choi, S. Zou, L. Kang, Effect of microneedle geometry and supporting substrate on microneedle array penetration into skin. *J. Pharm. Sci.* **102**, 4100–4108 (2013).

32. H.-H. Park, M. Seong, K. Sun, H. Ko, S. M. Kim, H. E. Jeong, Flexible and shape-reconfigurable hydrogel interlocking adhesives for high adhesion in wet environments based on anisotropic swelling of hydrogel microstructures. *ACS Macro Lett.* **6**, 1325–1330 (2017).

33. Q. Xu, A. Sigen, P. McMichael, J. Creagh-Flynn, D. Zhou, Y. Gao, X. Li, X. Wang, W. Wang, Double-cross-linked hydrogel strengthened by UV irradiation from a hyperbranched PEG-based trifunctional polymer. *ACS Macro Lett.* **7**, 509–513 (2018).

34. H.-H. Park, K. Sun, M. Seong, M. Kang, S. Park, S. Hong, H. Jung, J. Jang, J. Kim, H. E. Jeong, Lipid-hydrogel-nanostructure hybrids as robust biofilm-resistant polymeric materials. *ACS Macro Lett.* **8**, 64–69 (2019).

35. J. C. J. Wei, G. A. Edwards, D. J. Martin, H. Huang, M. L. Crichton, M. A. F. Kendall, Allometric scaling of skin thickness, elasticity, viscoelasticity to mass for micro-medical device translation: From mice, rats, rabbits, pigs to humans. *Sci. Rep.* **7**, 15885 (2017).

36. H. S. Gill, D. D. Denson, B. A. Burris, M. R. Prausnitz, Effect of microneedle design on pain in human volunteers. *Clin. J. Pain* **24**, 585–594 (2008).

37. E. Reyssat, Drops and bubbles in wedges. *J. Fluid Mech.* **748**, 641–662 (2014).

38. P. Renvoisé, J. W. M. Bush, M. Prakash, D. Quéré, Drop propulsion in tapered tubes. *Europhys. Lett.* **86**, 64003 (2009).

39. T. S. Kupper, R. C. Fuhlbrigge, Immune surveillance in the skin: Mechanisms and clinical consequences. *Nat. Rev. Immunol.* **4**, 211–222 (2004).

40. X. Chen, H. J. Corbett, S. R. Yukiko, A. P. Raphael, E. J. Fairmaid, T. W. Prow, L. E. Brown, G. J. P. Fernando, M. A. F. Kendall, Site-selectively coated, densely-packed microprojection array patches for targeted delivery of vaccines to skin. *Adv. Funct. Mater.* **21**, 464–473 (2011).

41. T. W. Prow, X. Chen, N. A. Prow, G. J. P. Fernando, C. S. E. Tan, A. P. Raphael, D. Chang, M. P. Ruutu, D. W. K. Jenkins, A. Pyke, M. L. Crichton, K. Raphaelli, L. Y. H. Goh, I. H. Frazer, M. S. Roberts, J. Gardner, A. A. Khromykh, A. Suhrbier, R. A. Hall, M. A. F. Kendall, Nanopatch-targeted skin vaccination against West Nile virus and Chikungunya virus in mice. *Small* **6**, 1776–1784 (2010).

42. E. Larrañeta, R. E. M. Lutton, A. D. Woolfson, R. F. Donnelly, Microneedle arrays as transdermal and intradermal drug delivery systems: Materials science, manufacture and commercial development. *Mater. Sci. Eng. R* **104**, 1–32 (2016).

43. J. B. Alarcon, A. W. Hartley, N. G. Harvey, J. A. Mikszta, Preclinical evaluation of microneedle technology for intradermal delivery of influenza vaccines. *Clin. Vaccine Immunol.* **14**, 375–381 (2007).

44. F.-S. Quan, Y.-C. Kim, A. Vunnava, D.-G. Yoo, J.-M. Song, M. R. Prausnitz, R. W. Compans, S.-M. Kang, Intradermal vaccination with influenza virus-like particles by using microneedles induces protection superior to that with intramuscular immunization. *J. Virol.* **84**, 7760–7769 (2010).

45. F.-S. Quan, Y.-C. Kim, R. W. Compans, M. R. Prausnitz, S.-M. Kang, Dose sparing enabled by skin immunization with influenza virus-like particle vaccine using microneedles. *J. Control. Release* **147**, 326–332 (2010).

46. M. Leone, J. Mönkäre, J. A. Bouwstra, G. Kersten, Dissolving microneedle patches for dermal vaccination. *Pharm. Res.* **34**, 2223–2240 (2017).

47. V. Baldo, T. Baldovin, G. Pellegrini, S. Majori, A. Floreani, M. C. Busana, C. Bertoncello, R. Trivello, Immunogenicity of three different influenza vaccines against homologous and heterologous strains in nursing home elderly residents. *Clin. Dev. Immunol.* **2010**, 517198 (2010).

48. M. R. Prausnitz, S. Mitragotri, R. Langer, Current status and future potential of transdermal drug delivery. *Nat. Rev. Drug Discov.* **3**, 115–124 (2004).

49. M. T. C. McCrudden, A. Z. Alkilani, A. J. Courtenay, C. M. McCrudden, B. McCloskey, C. Walker, N. Alshraiedeh, R. E. M. Lutton, B. F. Gilmore, A. D. Woolfson, R. F. Donnelly, Considerations in the sterile manufacture of polymeric microneedle arrays. *Drug. Deliv. Transl. Res.* **5**, 3–14 (2015).

50. E. M. Vicente-Pérez, H. L. Quinn, E. McAlister, S. O'Neill, L.-A. Hanna, J. G. Barry, R. F. Donnelly, The use of a pressure-indicating sensor film to provide feedback upon hydrogel-forming microneedle array self-application in vivo. *Pharm. Res.* **33**, 3072–3080 (2016).

51. J. J. Norman, J. M. Arya, M. A. McClain, P. M. Frew, M. I. Meltzer, M. R. Prausnitz, Microneedle patches: Usability and acceptability for self-vaccination against influenza. *Vaccine* **32**, 1856–1862 (2014).

52. J. J. Norman, M. R. Brown, N. A. Raviele, M. R. Prausnitz, E. I. Felner, Faster pharmacokinetics and increased patient acceptance of intradermal insulin delivery using a single hollow microneedle in children and adolescents with type 1 diabetes. *Pediatr. Diabetes* **14**, 459–465 (2013).

53. K. Mooney, J. C. McElnay, R. F. Donnelly, Children's views on microneedle use as an alternative to blood sampling for patient monitoring. *Int. J. Pharm. Pract.* **22**, 335–344 (2014).

54. J. C. Birchall, R. Clemo, A. Anstey, D. N. John, Microneedles in clinical practice—An exploratory study into the opinions of healthcare professionals and the public. *Pharm. Res.* **28**, 95–106 (2011).

55. R. Arnou, M. Frank, T. Hagel, A. Prébet, Willingness to vaccinate or get vaccinated with an intradermal seasonal influenza vaccine: A survey of general practitioners and the general public in France and Germany. *Adv. Ther.* **28**, 555–565 (2011).

56. M. R. Prausnitz, J. A. Mikszta, M. Cormier, A. K. Andrianov, in *Vaccines for Pandemic Influenza*, R. W. Compans, W. A. Orenstein, Eds. (Springer Berlin Heidelberg, 2009), pp. 369–393.

Citation: W.-G. Bae, H. Ko, J.-Y. So, H. Yi, C.-H. Lee, D.-H. Lee, Y. Ahn, S.-H. Lee, K. Lee, J. Jun, H.-H. Kim, N. L. Jeon, W. Jung, C.-S. Song, T. Kim, Y.-C. Kim, H. E. Jeong, Snake fang–inspired stamping patch for transdermal delivery of liquid formulations. *Sci. Transl. Med.* **11**, eaaw3329 (2019).

Science Translational Medicine

Snake fang–inspired stamping patch for transdermal delivery of liquid formulations

Won-Gyu Bae, Hangil Ko, Jin-Young So, Hoon Yi, Chan-Ho Lee, Dong-Hun Lee, Yujin Ahn, Sang-Hyeon Lee, Kyunghun Lee, Joonha Jun, Hyoung-Ho Kim, Noo Li Jeon, Woonggyu Jung, Chang-Seon Song, Taesung Kim, Yeu-Chun Kim and Hoon Eui Jeong

Bioinspired drug delivery

Topical formulations, transdermal patches, and microneedles can be used for drug delivery, avoiding the pain associated with hypodermic needle injections. Bae *et al.* developed flexible patches using microneedles to rapidly deliver liquid formulations through the skin. Inspired by rear-fanged snakes, the authors fabricated microneedles with open grooves that transdermally delivered dye-labeled proteinaceous solutions, liquid anesthetic, and a vaccine to guinea pigs and mice. Mice showed similar protection against influenza when immunized by microneedle patch or intramuscular injection. This flexible patch platform offers a versatile method of liquid drug delivery.

ARTICLE TOOLS	http://stm.sciencemag.org/content/11/503/eaaw3329
SUPPLEMENTARY MATERIALS	http://stm.sciencemag.org/content/suppl/2019/07/29/11.503.eaaw3329.DC1
RELATED CONTENT	http://stm.sciencemag.org/content/scitransmed/10/467/eaar2227.full http://stm.sciencemag.org/content/scitransmed/9/380/eaaf6413.full http://stm.sciencemag.org/content/scitransmed/7/300/300ra128.full
REFERENCES	This article cites 55 articles, 7 of which you can access for free http://stm.sciencemag.org/content/11/503/eaaw3329#BIBL
PERMISSIONS	http://www.sciencemag.org/help/reprints-and-permissions

Use of this article is subject to the Terms of Service